SIAM J. Applied Dynamical Systems
Vol. 5, No. 4, pp. 650–669

Motion Planning for an Articulated Body in a Perfect Planar Fluid*

Juan B. Melli†, Clarence W. Rowley†, and Dzhelil S. Rufat†

Abstract. Understanding fish-like locomotion as a result of internal shape changes may result in improved underwater propulsion mechanisms. We use a geometric framework to consider the simplified problem of an articulated two-dimensional body in a potential flow. This paper builds upon the current geometric theory by showing that although the group of Euclidean transformations is non-Abelian, certain tools available for Abelian groups may still be exploited, making use of the semidirect-product structure of this group. In particular, the holonomy in the rotation component may be explicitly computed as a function of the area enclosed by a path in shape space. We use this tool to develop open-loop gaits for an articulated body with two shape variables, using plots of the curvature of the mechanical connection, which relates motion in the shape space to motion of the overall body. Results from numerical computations of the mechanical connection are compared to theoretical results assuming the joints are hydrodynamically decoupled. Finally, we consider a simple method for trajectory tracking in the plane, using a one-parameter family of gaits.

Key words. geometric phase, locomotion, connection, principal bundle

AMS subject classifications. 81Q70, 53C29, 55R10

DOI. 10.1137/060649884

1. Introduction.

In this paper, we study articulated bodies in a potential flow and their locomotion as a result of internal shape changes. In particular, we seek to answer the following question: *Given a desired motion, what are the changes in shape that will achieve such a motion?*

Fish swimming has been studied for many decades in order to understand the physical mechanisms involved and ultimately to improve upon conventional methods of underwater propulsion. The interaction of solid bodies with an ideal fluid was first studied by Kirchhoff in the 1870's [7, 9]. In the 1960's, analytical models by Wu examined the swimming of a two-dimensional flexible plate with a small amplitude traveling wave [24, 25], while Lighthill considered the propulsion of slender-body fishes [12, 13, 14, 15]. More recently, Kelly [5, 6] studied the self-propulsion of fish-like and amoeba-like swimmers in potential and Stokes flow from a geometric point of view, by viewing the configuration space as a principal fiber bundle, in which the base space consists of the internal shape variables, and the fibers are the group of rigid motions of the overall body. The motion along the fiber is related to the motion in the base space by a principal connection, called the *hydromechanical connection*, a term which comes from the geometric mechanics community [19]. These techniques were used in [8] to study geometric phases in articulated free rigid bodies, and similar techniques

*Received by the editors January 13, 2006; accepted for publication (in revised form) by L. Fauci August 17, 2006; published electronically November 22, 2006. This work was supported by the National Science Foundation (award CMS-0347239, with support from an REU supplement) and an NDSEG Graduate Research Fellowship.
http://www.siam.org/journals/siads/5-4/64988.html
†Mechanical Engineering Department, Princeton University, Princeton, NJ 08544 (jmelli@princeton.edu, cwrowley@princeton.edu, drufat@princeton.edu).

were used in [21, 23] to study the motion of deformable bodies and articulated rigid bodies in a fluid, assuming small amplitude motions, and assuming that the individual links were *hydrodynamically decoupled*; that is, that the added inertia of each link is independent of the position or velocity of the other links. Kanso et al. [4] later formulated the potential flow problem explicitly as a reduction by stages [1] (although such a formulation was already implicit in [5]) and accurately computed the added inertia terms using a boundary element method. Tools from control theory and geometric mechanics have also been used to generate gaits for locomotion of underwater vehicles [11, 21, 22].

Benefits of the geometric formulation. One of the advantages of formulating the equations using the structure of a fiber bundle is that one may use the hydromechanical connection to design swimming gaits to achieve desired motions. In this paper, we use the formulation of [5, 4] to develop open-loop swimming gaits to achieve arbitrary rotations in two dimensions. The technique we use is well known for Abelian groups; we show that they may also be used for the rotation component of the Euclidean group, exploiting the semidirect product structure $SE(2) = SO(2) \circledS \mathbb{R}^2$, since $SO(2)$ is Abelian. Whereas some previous results were limited to small amplitude gaits or assumed hydrodynamically decoupled links, our results allow us to develop finite amplitude gaits and accurately compute the motion. By numerically computing the curvature of the hydromechanical connection, it becomes possible to develop such gaits by inspection.

It is well known that fish propulsion relies in part on the shedding of vorticity, for instance, as demonstrated in the experiments of [3]. Although we ignore the effects of viscosity and do not model vortex shedding, our model captures the inertial forces associated with fish-like swimming, which are most important during quick maneuvers. In other words, our model is not valid as representative of real fish swimming unless maneuvers are performed quickly. We consider this to be a first step at developing fish-like gaits and plan to incorporate the effects of vorticity in future models.

This paper is organized as follows. In section 2 we introduce the problem of a three-link fish-like articulated swimmer in a potential flow. Section 3 includes the geometric framework necessary to study the present problem and includes a formula for computing the holonomy in a semidirect product group $S = G \circledS V$, where G is an Abelian group and V is a vector space. This theory is applied in section 4 to find open-loop gaits from plots of the curvature of the local connection to achieve a desired net rotation in the fish-like body. For the three-link geometry, it is found that the most efficient turning gaits involve motions where the body is "C"-shaped, rather than "S"-shaped. Further, we investigate different shape geometries for maneuvering, including the effect of removing the middle link. The curvature plots are compared to the case where the links are assumed to be hydrodynamically decoupled. We then show how the curvature plots can be used to generate small-amplitude gaits for the non-Abelian group components. Finally, in section 5 we consider a family of gaits and present a method for following a trajectory in the plane.

2. Problem formulation.

Consider a fish-like body modeled as a set of articulated rigid links connected by hinged joints. The body is assumed to be two-dimensional and neutrally buoyant. The example we will consider here is a three-link body with two joints, as in Figure 1, which begins at rest, and is immersed in a perfect fluid. The formulation we use is the same

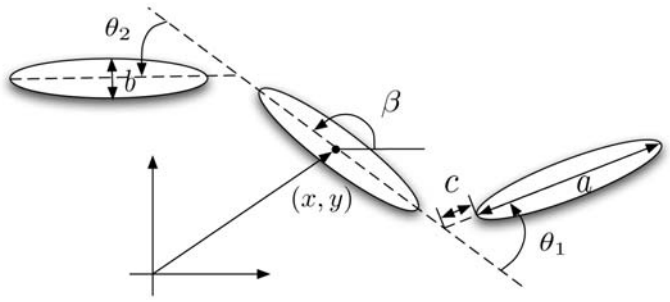

Figure 1. *A three-link swimmer.*

as that in [4], but here we review the main ideas and define the notation used.

Kinematics. The overall motion of the body is represented by the position and orientation of the middle body relative to an inertial frame of reference and is given by an element $s = (x, y, \beta) \in SE(2)$, the special Euclidean group. As noted earlier, we will exploit the semidirect product structure of this group. The shape of the body is determined by the angles θ_1 and θ_2 between the joints, which we call the shape variables. In computations, it will be useful to express the positions of the outer links relative to this middle link by elements $x_1, x_2 \in SE(2)$, where we label the outer links as 1 and 2 as in Figure 1. These elements x_1 and x_2 are of course determined completely by the angles θ_1 and θ_2.

Dynamics. The lack of external forces or torques acting on the body or the fluid leads to the conservation of a momentum-like quantity of the body plus fluid system. We assume the fluid is inviscid, incompressible, and because there is no mechanism for the generation of vorticity, irrotational for all time. Thus the velocity field can be represented as the gradient of a scalar potential,

$$\mathbf{u} = \nabla\phi. \tag{2.1}$$

To determine the equations of motion, we use the Lagrangian formulation, as in [9, 5, 4]. The Lagrangian of the system is equal to the total kinetic energy of the body plus the fluid,

$$L = T_{\mathcal{B}} + T_{\mathcal{F}}, \tag{2.2}$$

where the fluid kinetic energy $T_{\mathcal{F}}$ is given by

$$T_{\mathcal{F}} = \frac{1}{2}\int_{\mathcal{F}} \rho_{\mathcal{F}} |\mathbf{u}|^2 \, \mathrm{d}V, \tag{2.3}$$

where $\rho_{\mathcal{F}}$ is the fluid density. For an ideal fluid, it is well known that the motion of the fluid is determined completely by the motion of the solid bodies [9]; that is, the total kinetic energy may be expressed solely in terms of the velocities of the bodies, with the role of the fluid appearing only as added inertias that of course depend on the configuration of the solid bodies. This formulation is originally due to Kirchhoff [7, 9] and may also be understood as an explicit reduction by the particle-relabeling symmetry [4].

The potential ϕ may therefore be written as a sum of translational and rotational velocity potentials corresponding to each link. The Neumann boundary condition of no penetration is imposed along the surface, requiring that the normal velocity of the fluid, $\nabla\phi \cdot \mathbf{n} = \frac{\partial \phi}{\partial \mathbf{n}}$, at a point along the body surface be equal to the normal velocity of the body at that point.

Since the fluid has infinite extent, the total momentum of the system is indeterminate. However, we may consider the system "impulse," a momentum-like quantity defined by Lord Kelvin [9]. The impulse is a product of the total link inertias (actual plus added inertias) and the body velocities of each link, and may be expressed as in [4] as

$$h_s = \sum_{j=1}^{3} \Big(\mathrm{Ad}^T_{x_1^{-1}}(\mathbb{I}_{1j}\xi_j) + \mathrm{Ad}^T_{x_2^{-1}}(\mathbb{I}_{2j}\xi_j) + \mathbb{I}_{3j}\xi_j \Big), \tag{2.4}$$

where $\xi_j \in \mathbb{R}^3 \cong \mathfrak{se}(2)$ is the velocity of link j with respect to a reference frame attached to that link, where links $1, 2$ are the outer links as before, and link 3 is the middle link. The matrices $\mathbb{I}_{ij}$ are the total inertia terms such that the total kinetic energy of the body plus fluid system is

$$T = \frac{1}{2} \sum_{i,j=1}^{3} \xi_i^T \mathbb{I}_{ij} \xi_j \tag{2.5}$$

and $\mathrm{Ad}^T_{x_j^{-1}}$ are operators that map the momenta term corresponding to body j from the j body-fixed frame to the body-fixed frame of the middle body (see [17, 4] for more discussion of the Ad operator and background on Lie groups). Defining $\zeta_j = x_j^{-1}\dot{x}_j$ as the velocity of link j relative to the middle link, expressed with respect to a frame fixed to body j, we then can write the velocities ξ_j as

$$\xi_j = \zeta_j + \mathrm{Ad}_{x_j^{-1}}\xi_3, \quad j = 1, 2. \tag{2.6}$$

The system impulse may also be expressed with respect to an inertial frame, in which case it will remain unchanged due to the lack of external forces and moments. As currently defined with respect to the body frame, in general, the value will change in time. However, when the system begins at rest, the system impulse h_s remains zero for all time. In this case, (2.4) combined with (2.6) can be rewritten as

$$\mathbb{I}_{\mathrm{loc}}\,\xi_3 + \sum_{\alpha,\beta=1}^{2} \big(\mathrm{Ad}^T_{x_\alpha^{-1}} \mathbb{I}_{\alpha\beta} + \mathbb{I}_{3\beta} \big) \zeta_\beta \;=\; 0, \tag{2.7}$$

where

$$\mathbb{I}_{\mathrm{loc}} \;=\; \sum_{\alpha,\beta=1}^{2} \Big(\mathrm{Ad}^T_{x_\alpha^{-1}} \mathbb{I}_{\alpha\beta} \mathrm{Ad}_{x_\beta^{-1}} + \mathrm{Ad}^T_{x_\alpha^{-1}} \mathbb{I}_{\alpha 3} + \mathbb{I}_{3\beta} \mathrm{Ad}_{x_\beta^{-1}} \Big) + \mathbb{I}_{33} \tag{2.8}$$

is the locked moment of inertia. We may then write (2.7) as

$$\mathbb{I}_{\mathrm{loc}} \big(\xi_3 + \mathcal{A}(x)\dot{x} \big) = 0, \tag{2.9}$$

where $\mathcal{A}$ is the local form of the mechanical connection, an $\mathfrak{se}(2)$-valued one-form on the shape space. When the locked moment of inertia is nondegenerate, (2.9) simplifies to $\xi_3 + \mathcal{A}(x)\dot{x} = 0$. Due to the constraint on the joint between the links, the rigid motion x_α can be parameterized by the single variable θ_α. Also, considering that $\xi_3 = g^{-1}\dot{g}$, the equations of motion for the system can be written as

$$\dot{s}(t) = -T_e L_{s(t)} \left(\mathcal{A}(\theta)\dot{\theta}(t) \right) \tag{2.10}$$

or in shorthand notation

$$\dot{s} = -s\mathcal{A}(\theta)\dot{\theta}, \tag{2.11}$$

where $s \in S$, $\mathfrak{s} = T_e S$, and $\mathcal{A} : TQ \to \mathfrak{s}$ is the (local) *mechanical connection*, a Lie algebra-valued one form on the shape space. It maps a prescribed shape velocity element $\dot{\theta} = (\dot{\theta}_1, \dot{\theta}_2)$ to the negative of the body velocity of the middle body, an element of $\mathfrak{se}(2)$. The connection is a function of the added inertias and is computed numerically at each time step. The motion of the fish can be solved by prescribing a path for θ in shape space and integrating equation (2.10) in time. Trial and error was used in [4] to determine gaits which generate forward and turning motions. Here, we ask the reverse question: *Given a desired motion, what is the closed path in shape space required to achieve this motion?*

3. Holonomy in semidirect product groups. If the group S is Abelian, then for a given path in shape space given by $\theta(t)$, $t \in [0, 1]$, the solution to (2.11) with initial condition $s(0) = e$ is simply

$$s(1) = \exp\left(-\int_0^1 \mathcal{A}(\theta)\dot{\theta}(t)\, dt \right). \tag{3.1}$$

If $\theta(t)$ is a closed path for $t \in [0, 1]$, then this result is equivalent to integrating the connection along this path in shape space, or by the Stokes theorem, to integrating the curvature of the connection over the area enclosed by the path,

$$\exp\left(-\int_0^1 \mathcal{A}(\theta)\dot{\theta}(t)\, dt \right) = \exp\left(-\int_{\partial C} \mathcal{A}(\theta)\, \mathrm{d}\theta \right) = \exp\left(-\iint_C \mathrm{D}\mathcal{A}(\theta)\, \mathrm{d}A \right), \tag{3.2}$$

where the curvature $\mathrm{D}\mathcal{A} : T_qQ \times T_qQ \to \mathfrak{s}$ is the covariant derivative of the connection $\mathcal{A}$, given by

$$\mathrm{D}\mathcal{A}(X, Y) = d\mathcal{A}(X, Y) - [\mathcal{A}(X), \mathcal{A}(Y)], \tag{3.3}$$

where X, Y are vector fields on Q [20]. This is a powerful result because it greatly simplifies the problem of generating gaits to achieve a desired motion. First, one selects the desired element in the group space and solves for the right-hand side of (3.1) by taking the logarithm of both sides. Then, using the equality in (3.2), one finds an area in shape space that encloses the corresponding volume of the curvature of the connection.

Unfortunately, the case when S is non-Abelian has no explicit solution. This is the case for motion in the plane, where the Lie group is $S = SE(2)$. However, $SE(2)$ can be expressed

as the semidirect product $SO(2)\circledS\mathbb{R}^2$. When the Lie group component (G) of the semidirect product group is Abelian, it can be shown that the solution for this component of the semidirect product group is the same as that for the Abelian case (3.1).

Semidirect products. Recall that if G is a Lie group that acts on a vector space V, then one can define the semidirect product $G\circledS V$ as the usual product, with the group operation $(g_1, v_1)(g_2, v_2) = (g_1g_2, g_1v_2+v_1)$, where $g_1, g_2 \in G$, $v_1, v_2 \in V$. The Lie algebras corresponding to the various groups are $\mathfrak{g} = T_eG$, $V = T_eV$, and $\mathfrak{s} = T_eS$.

Theorem 3.1. *Let $S = G\circledS V$, where G is Abelian. Consider a closed curve $\theta(t) \in Q$ for $t \in [0, 1]$, and let $\mathcal{A} : TQ \to \mathfrak{s}$ be a principal connection with components $\mathcal{A}_\mathfrak{g} : TQ \to \mathfrak{g}$ and $\mathcal{A}_V : TQ \to V$. Then if $s(t) = (g(t), v(t)) \in S$ satisfies*

$$\dot{s} = -s\mathcal{A}(\theta)\dot{\theta} \tag{3.4}$$

with $s(0) = (e, 0)$, then

$$\text{holonomy}_G := g(1) = \exp\left(-\int_{\partial C} \mathcal{A}_\mathfrak{g}\, d\theta\right) = \exp\left(-\iint_C \mathrm{D}\mathcal{A}_\mathfrak{g}\, dA\right). \tag{3.5}$$

Proof. Since $\theta(t)$ is given, we may rewrite (3.4) as $\dot{s} = -s\xi(t)$, where $\xi = \mathcal{A}(\theta)\dot{\theta}$ is given. Writing $\xi = (\xi_g, \xi_v)$, where $\xi_g \in \mathfrak{g}$ and $\xi_v \in V$, this becomes (see [18])

$$\dot{g} = -T_eL_g\xi_g, \tag{3.6}$$

$$\dot{v} = -\rho(g)\xi_v. \tag{3.7}$$

Clearly, (3.6) is decoupled from (3.7), and since G is Abelian, the solution is

$$g(t) = \exp\left(-\int_0^t \xi_g(\tau)d\tau\right). \tag{3.8}$$

The holonomy of S in the G component is then

$$\text{holonomy}_G = g(1) = \exp\left(-\int_{\partial C} \mathcal{A}_\mathfrak{g}\, d\theta\right) = \exp\left(-\iint_C \mathrm{D}\mathcal{A}_\mathfrak{g}\, dA\right),$$

where the last equality is by the Stokes theorem. ∎

This result is used to generate gaits for the Abelian component of the Lie group which correspond to turning maneuvers for the fish. As demonstrated in Figure 6(a), this result does not apply in the general case, and we cannot use this method to generate finite amplitude translational gaits.

4. Results.

For the fish-like body depicted in Figure 1, the shape space Q is parameterized by (θ_1, θ_2), so the local connection $\mathcal{A}(\theta_1, \theta_1) : T_{(\theta_1,\theta_2)}Q \to \mathfrak{se}(2)$ is a Lie-algebra-valued one-form on Q, which may be written as

$$\mathcal{A}(\theta_1, \theta_2) = f(\theta_1, \theta_2)\mathrm{d}\theta_1 + g(\theta_1, \theta_2)\mathrm{d}\theta_2, \tag{4.1}$$

where $f, g : Q \to \mathfrak{se}(2)$ depend on the added inertia terms, which depend on the shape of the body and are computed from (2.9). A boundary element method using source distributions is

employed to compute the added inertia terms at each time step. For details of the computation, see [4]. The curvature $D\mathcal{A}$ is then a Lie-algebra-valued two-form on Q, computed from (3.3) as

$$D\mathcal{A} = \left[\left(\frac{\partial g}{\partial \theta_1} - \frac{\partial f}{\partial \theta_2}\right) - [f, g]\right] \mathrm{d}\theta_1 \wedge \mathrm{d}\theta_2 \tag{4.2}$$

$$= \gamma(\theta_1, \theta_2)\mathrm{d}\theta_1 \wedge \mathrm{d}\theta_2, \tag{4.3}$$

where $\gamma : Q \to \mathfrak{se}(2)$ is the bracketed term in (4.2). The curvature has three components: one corresponding to rotational body velocity and two corresponding to translational body velocity terms. The translational components, denoted u and v, correspond to motion parallel to the direction of the major and minor axes of the middle link, respectively. The three components of γ are computed numerically on a grid in the (θ_1, θ_2) plane and plotted in Figure 2. The plots correspond to a fish-like body with three equal size elliptical links where the dimensions (as in Figure 1) are $a = 20$, $c = 2$ and the aspect ratio of the ellipses is 10.

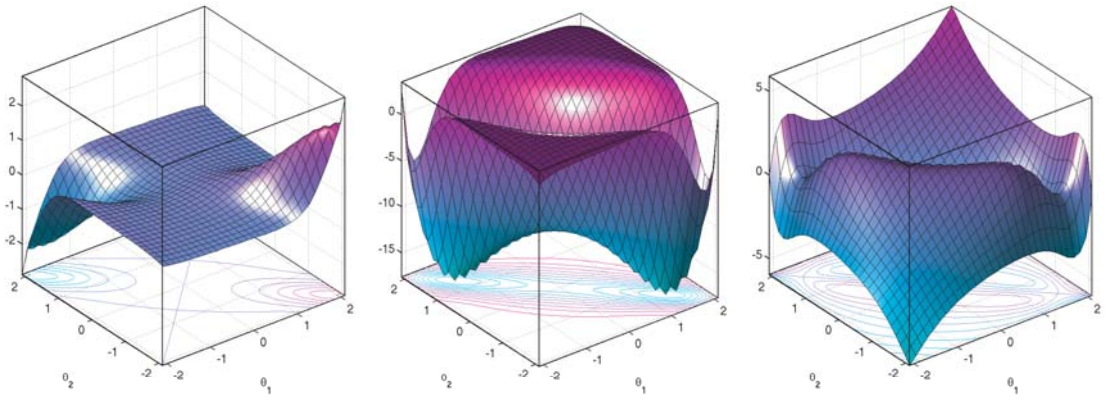

(a) (b) (c)

Figure 2. (a) ω, (b) u, *and* (c) v *components of curvature.*

4.1. Using the curvature for gait generation. Since $SO(2)$ is Abelian and $SE(2) = SO(2) \circledS \mathbb{R}^2$, one can use the ω component of the curvature plot to develop finite-amplitude turning gaits, using the theory in section 3. The ω-component plot is shown enlarged in Figure 4. Note that the regions of largest curvature occur in two opposite corners of the shape space. These regions correspond to the fish configuration where the joints are bent in a "C"-shape. The most efficient turning gaits will enclose these regions of high curvature. Intuitively, this makes sense as one would expect a turning fish to coil its body into a "C"-shape to minimize the inertial resistance of the fluid as it turns. Likewise, a fish in an extended or "S"-shape configuration trying to rotate would encounter larger inertial forces and would not be expected to turn easily.

The procedure for gait-generation for the Abelian subgroup component is straightforward:

1. Choose the desired Abelian Lie group element (here, the desired net rotation).

2. Determine the corresponding Lie algebra element by applying the logarithm map.
3. Find a path in shape space that encloses a volume equal to the negative value of the Lie algebra element found in the previous step.

Note that, since the net rotation depends only on the enclosed area, the initial shape configuration need not be a point on the path, as shown in Figure 3.

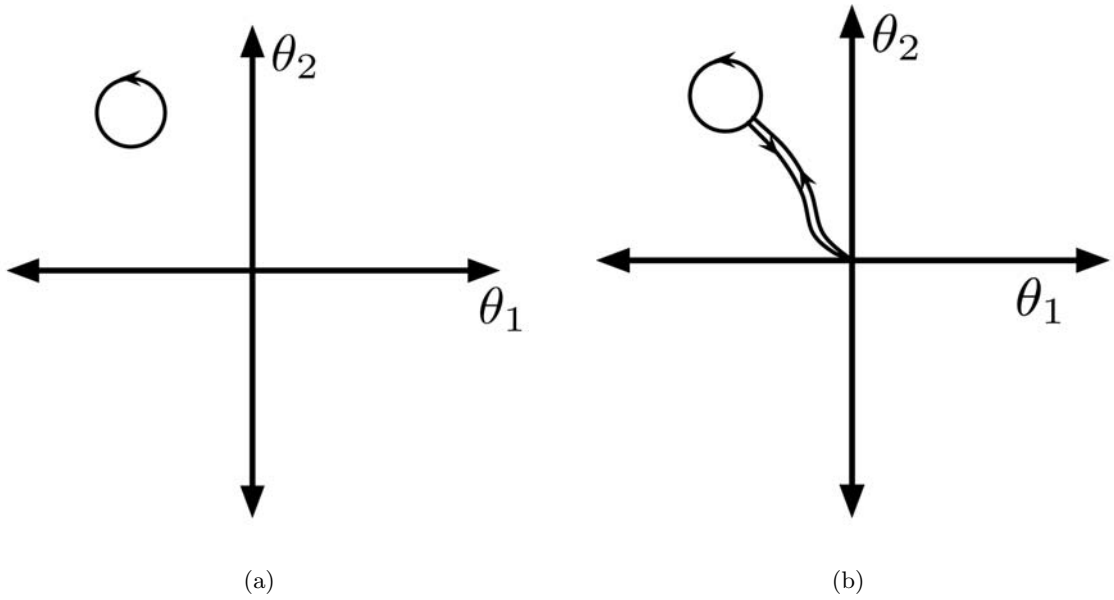

(a) (b)

Figure 3. *Two paths resulting in the same holonomy in the Abelian subgroup component, but starting and ending at different points in shape space.*

Exponential map. The exponential map takes elements of the Lie algebra and maps them to the Lie group. For $SE(2)$, the exponential map is given by $\exp(u, v, \omega) = (x, y, \beta)$, where

$$\beta = \omega, \tag{4.4}$$

$$(x, y) = \begin{cases} (u, v), & \omega = 0, \\ \frac{1}{\omega}(u \sin\omega + v(1 - \cos\omega), u(\cos\omega - 1) + v \sin\omega), & \omega \neq 0. \end{cases} \tag{4.5}$$

For the purposes of this paper, we will require only the component of this map given by (4.4), so for this component, the exponential map, and its inverse, the log map, are just the identity.

As an example of gait-generation, we choose a desired net rotation of $\beta = \pi/4$. Thus, $\omega = \pi/4$ and we seek a closed path in (θ_1, θ_2) space that encloses a volume equal to $-\pi/4$. Figure 4 illustrates one such path, given by

$$\begin{aligned} \theta_1(t) &= -1.5 + .46\cos(t), \\ \theta_2(t) &= 1.5 - .46\sin(t), \end{aligned} \tag{4.6}$$

where $t \in [0, 2\pi]$. Note that the holonomy is independent of the speed of travel along this path.

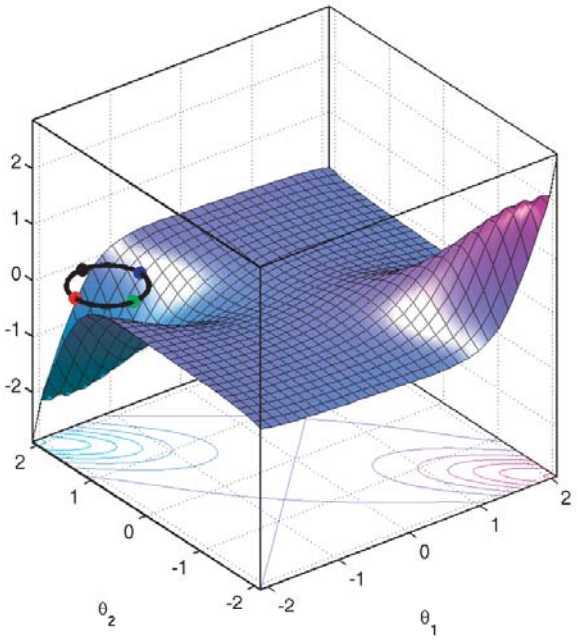

Figure 4. *Path in shape space resulting in net rotation of* $\frac{\pi}{4}$ *radians:* $\theta_1(t) = -1.5 + .46\cos(t)$*;* $\theta_2(t) = 1.5 - .46\sin(t)$.

The fish middle link begins at a zero degree angle from the horizontal and, after one shape space loop, has rotated 45 degrees counterclockwise, as in Figure 5. The angles of the joints are the same in the original and final configuration.

The start and end points of the closed path have no effect on the net rotation, as implied by (3.5). However, the choice for the start and end points will affect the net holonomy in the translational component of motion. Figure 6 shows the trajectory of the center of the fish for various starting points in the prescribed path. The starting points are labeled in Figure 4 in the same color as the corresponding paths in Figures 6(a) and 6(b). In each case, the path is in the clockwise direction. Because the net holonomy in these directions depends on the starting point of the path, it is clear that for the translational component in $SE(2)$, as is the case for general non-Abelian groups, a formula analogous to (3.5) is not possible, as the holonomy cannot depend only on the area enclosed by the path.

As a second example, we present a gait to achieve a net rotation of $\pi/2$, while starting and ending with the fish in a straight configuration (unlike the previous example, where the fish starts and ends in a "C"-shape). In order to begin and end with a straightened out configuration, we choose the gait shape space path to begin and end at the origin, and numerically find an area in shape space that encloses a volume of $-\pi/2$. The path selected is shown in red in Figure 7 along with the initial and final configurations of the swimmer. A video animation of the turning gait is available.

4.2. Determining degree of maneuverability of fish shape via numerical experiments. A numerical study was performed to determine how the body geometry affects the rotational

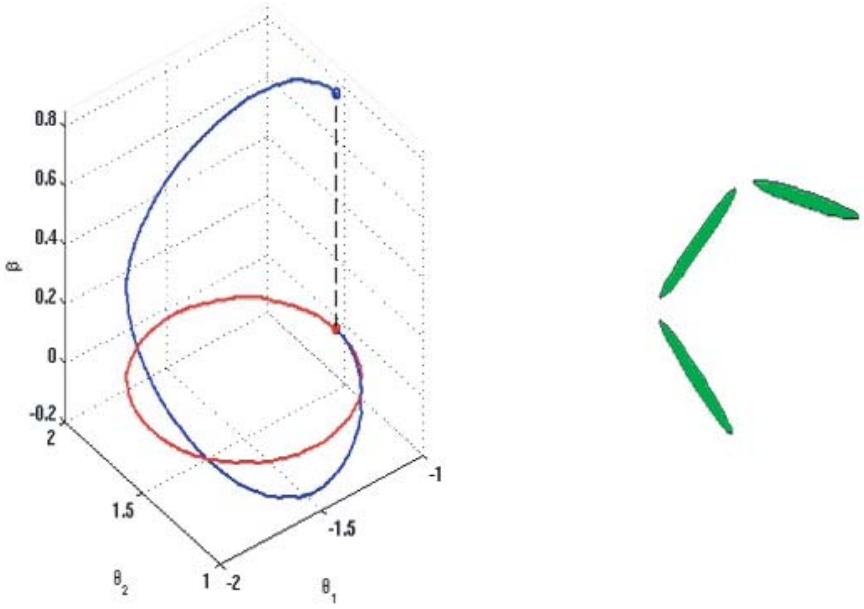

Figure 5. *Turning gait path in shape space in red with the rotation holonomy in blue along with the final configuration for a three-link swimmer after one turning gait. See also the accompanying animation* (64988_01.gif [190KB]).

maneuverability of the fish. This was done by examining the ω component of the curvature plots for various shape geometries along the line $\theta_1 = -\theta_2$, corresponding to "C"-shapes, which have been shown to be the most efficient configurations for turning gaits. The variables examined were the aspect ratio of each individual ellipse as well as the gap between the joints. The number of bodies was held fixed at three and the sizes of all three bodies are assumed to be equal. It was found (see Figure 8(b)) that a larger aspect ratio cross section results in a larger curvature for a given shape configuration. Also, as illustrated in Figure 8(a), increasing the gap between joints improves the maneuverability as well, though the effect saturates for larger gap values. Thus for improved turning, a slender fish with large gaps between joints is preferred to a rounder body with the individual links close together.

4.3. Hydrodynamically coupled versus decoupled. The swimming of an articulated body in a potential flow has been studied by Radford [22], in which it was assumed that the bodies were dynamically coupled, but hydrodynamically decoupled; that is, the added inertias for each body component are determined assuming it is hydrodynamically isolated from all the other bodies. Our current numerical scheme removes this approximation and accurately computes the added inertias of the system, and thus provides a way of validating the hydrodynamically decoupled assumption.

We compare the curvature plots for both the hydrodynamically coupled and decoupled cases. Figure 9 is a plot of the ω component of the curvature for both cases. The plots are qualitatively similar in many respects: both show relatively small curvature in the areas of shape space corresponding to the fish in an "S" configuration. Likewise, the decoupled case accurately predicts that the curvature is greatest when the fish is in a "C" configuration.

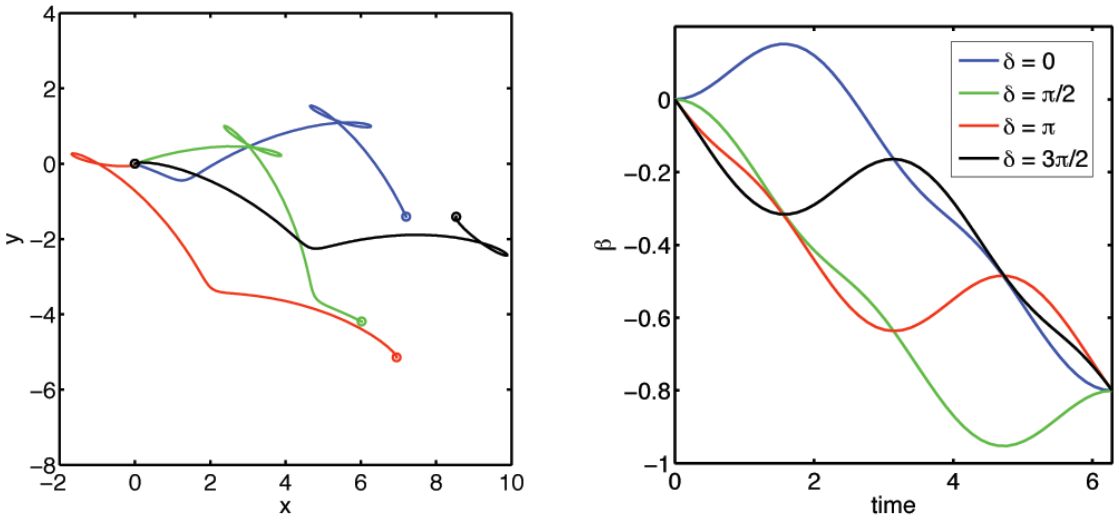

(a) (b)

Figure 6. *Group motion:* (a) *Translation and* (b) *rotation resulting from the prescribed paths in shape space:* $\theta_1(t) = -1.5 + .46\cos(t+\delta)$; $\theta_2(t) = 1.5 - .46\sin(t+\delta)$ *for various values of* δ. *The start and end points of the closed path have no effect on the net rotation but do affect the net holonomy in the translational component. Because the net translational holonomy depends on the starting point of the path, a formula analogous to* (3.5) *is not possible, as the holonomy cannot depend only on the area enclosed by the path.*

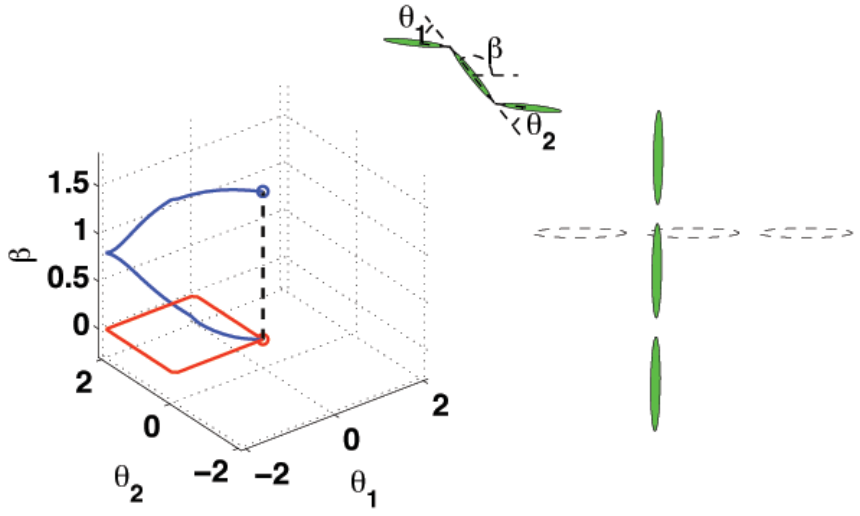

Figure 7. *Turning gait path in shape space in red with the rotation holonomy in blue along with the initial (dotted) and final (solid) configurations for a three-link swimmer after one turning gait. See also the accompanying animation* (64988_02.gif [138KB]).

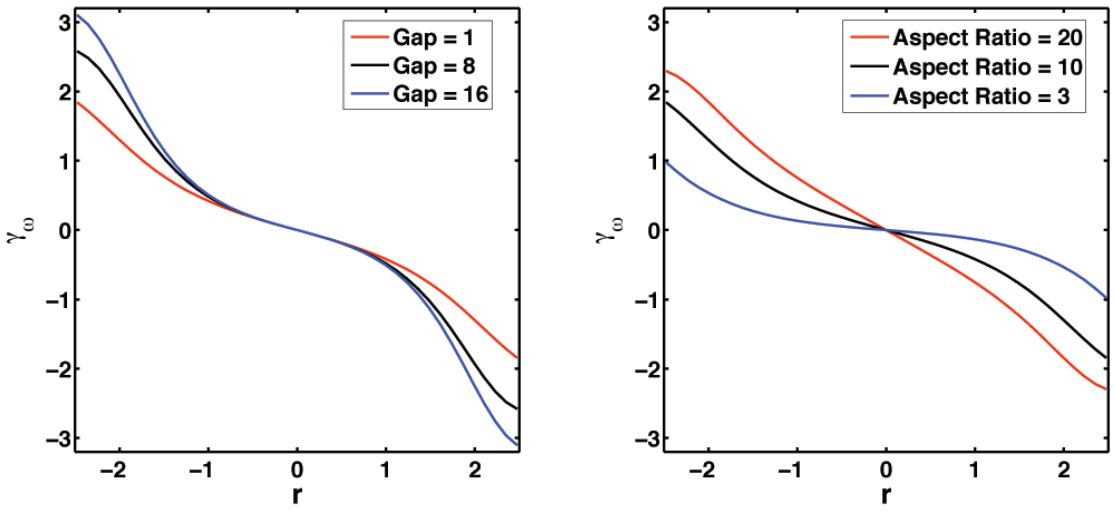

(a) (b)

Figure 8. *Parametric study of various fish geometries. r is the distance from the origin along the line $\theta_1 = -\theta_2$:* (a) *The gap between links is varied, while the aspect ratio is held fixed at a value of* 10. (b) *The aspect ratio of each link is fixed. The gap and overall length of the fish are held fixed.*

However, the decoupled assumption incorrectly predicts a maximum curvature when the joints are at approximately $\pm\pi/2$. Also, the decoupled assumption underpredicts the curvature in the highest curvature region. However, overall the hydrodynamically decoupled assumption is surprisingly accurate at predicting curvature of the connection, and thus predicting the overall rotation for any given gait.

4.4. Removing the middle link. It has been observed that carangiform fish have developed a narrow necking region in the peduncle, the region anterior of the tail (see Figure 10). Lighthill has proposed that the reduced added mass in this region minimizes the recoil forces experienced by a fish [13]. We crudely model this necking region and reduction in size by removing the middle link and studying the effect on the maneuverability of the fish.

Consider the same three-link, two hinged swimmer as before, but now with the middle link removed, as in Figure 11. Here, the front link can be thought of as representing the dorsal fin, and the rear link as representing the caudal fin in a carangiform fish. (The interactions of these fins in real fishes were considered in the experiments of [2]. For more on undulatory propulsion in carangiform fishes, see [10].) The curvature plots for the two-link swimmer are shown in Figure 12. They are qualitatively similar to those of the three-link swimmer; however they are quantitatively considerably different. The ω-component plot, Figure 12(a), has some characteristics similar to those of the three-link ω curvature plot—most notably a relatively flat surface, except in the two shape space regions corresponding to a "C" type configuration in the three-link body. Unlike the three-link plot, however, the two-link plot has a local maximum in the high curvature region. This is similar to what was found in the case of

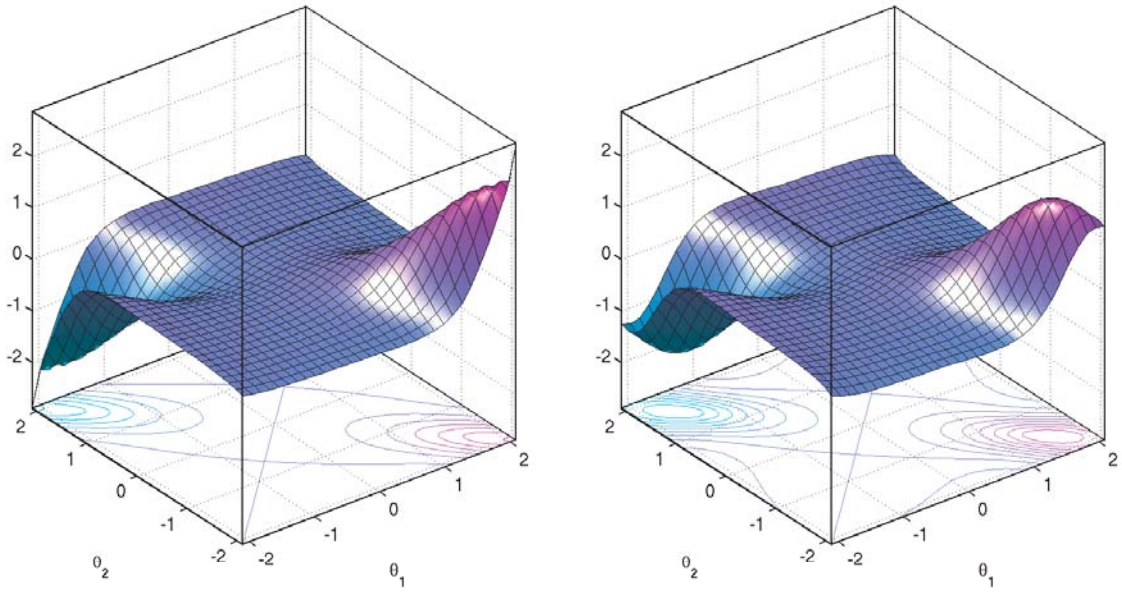

Figure 9. (a) *Hydrodynamically coupled and* (b) *hydrodynamically decoupled* ω *component of curvature plot.*

Figure 10. *Bluegill Sunfish (Lepomis macrochirus), a carangiform mode swimmer. Notice the narrow necking region between the body and tail. (Photo courtesy George Lauder, Harvard University.)*

the hydrodynamically decoupled three-link body. Perhaps the lack of a middle link and thus increased distance between links improves the assumption of hydrodynamic isolation which results in the similarity between these two figures. As a clearer example of this effect, consider the ω-component curvature plots in Figure 13 for the two-link body under the assumption of

Figure 11. *A two-link swimmer. The two links may be viewed as representing the dorsal and caudal fins of a carangiform swimmer.*

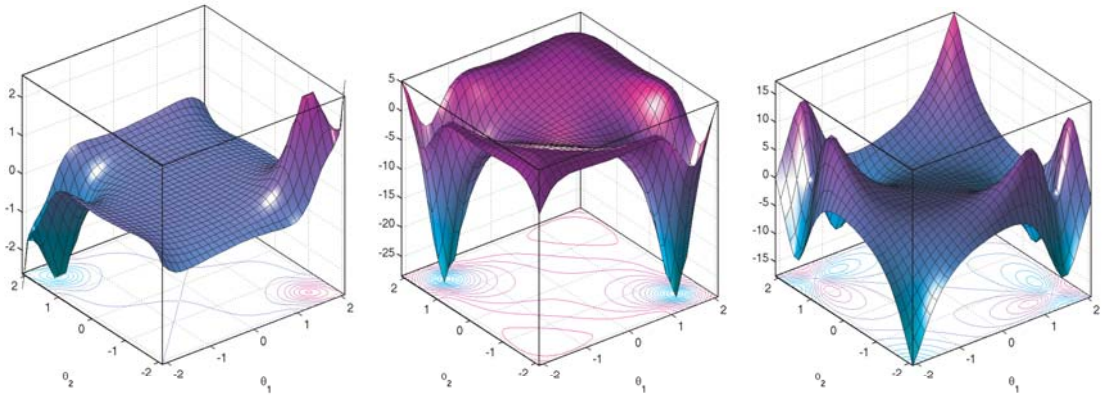

(a) (b) (c)

Figure 12. (a) ω, (b) u, *and* (c) v *components of curvature for a two-link, two hinge body assuming hydrodynamically coupled links.*

both hydrodynamically coupled and hydrodynamically decoupled links. The curvature plots for both cases are qualitatively and quantitatively very similar.

Finally, for a more direct comparison, Figure 14 shows the ω curvature component for the three-link body versus that of the two-link body (both under the assumption of hydrodynamically coupled links) along the cross section defined by the line $\theta_1 = -\theta_2$. The curvature value is plotted as a function of distance r from the origin. We see that for a body that is restricted to small angular deformations, the three-link configuration is preferred to the two-link configuration. A body that is able to achieve larger angular displacements of its joints may prefer the two-link configuration over the three-link configuration, as it allows for increased rotational maneuverability for some gaits. For example, for the same path prescribed in (4.6), the net holonomy for the two-link body is 0.99 radians, compared to 0.79 radians for the three-link body.

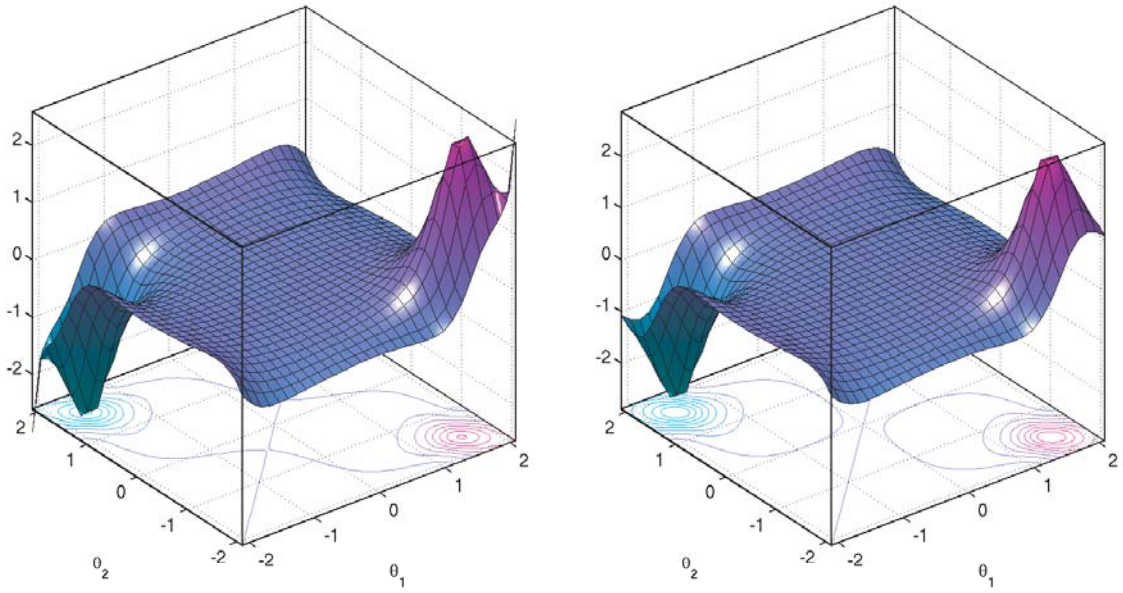

Figure 13. (a) *Hydrodynamically coupled and* (b) *hydrodynamically decoupled* ω *component of curvature for a two-link body.*

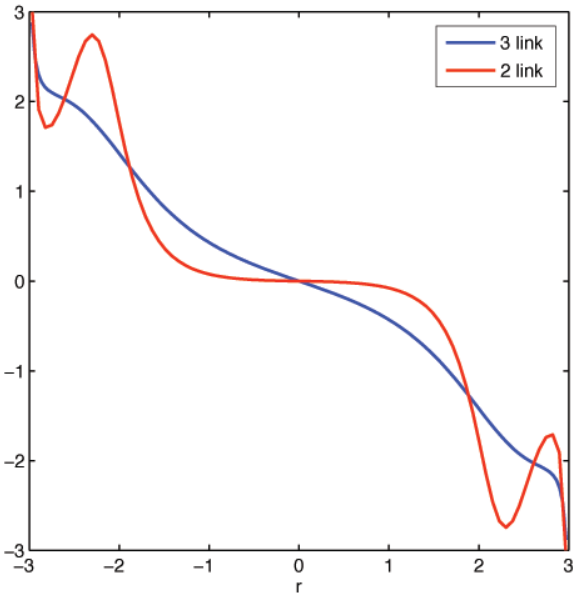

Figure 14. *Comparison of the* ω *curvature component versus distance from the origin along a line defined by* $\theta_1 = -\theta_2$ *for a two-link and three-link body.*

4.5. Trajectory generation. As noted in section 3 and illustrated in Figure 6(a), Theorem 3.1 cannot be applied to the vector space component of a semidirect product group, so curvature plots cannot be used to develop large-amplitude gaits for translation in the plane. However, the curvature plots can be used to develop small-amplitude gaits to achieve local trajectory tracking.

Using the Magnus expansion [16], Radford [23] obtained a local expansion of the group displacement resulting from a closed path α in shape space for systems in the form of (2.11) where the connection $\mathcal{A}$ is a function of the shape variables. The expansion, to third order, is

$$z(\alpha) = -\frac{1}{2}F_{ij}\int_\alpha d\theta^i d\theta^j + \frac{1}{3}(F_{ij,k} - [\mathcal{A}_i, F_{jk}])\int_\alpha d\theta^i d\theta^j d\theta^k + \dots, \tag{4.7}$$

where F_{ij} is the curvature of $\mathcal{A}$,

$$F_{ij} \equiv \mathcal{A}_{j,i} - \mathcal{A}_{i,j} - [\mathcal{A}_i, \mathcal{A}_j], \tag{4.8}$$

which is equivalent to (4.3), and the subscript j represents differentiation with respect to θ_j. F and $\mathcal{A}$ are evaluated at the starting point on the path. The coefficient of the first term is proportional to the local curvature value. Thus, for small-amplitude loops in shape space, the curvature plots can be used to develop gaits. The coefficient of the next term is a function of the local connection and curvature values as well as a higher order derivative of the curvature. This term is nonzero for 2:1 Lissajous-type paths in shape space. Assuming the system is controllable with up to second order bracket motions, (4.7) can be used to determine 1:1 and 2:1 small-amplitude Lissajous-type gaits to achieve the desired trajectory in the group.

Note also that small-time local controllability for the system can be shown from the Lie algebra rank condition. One checks numerically that the vector fields of the local connection plus iterated Lie brackets of those vector fields span the Lie algebra $\mathfrak{se}(2)$ at each point in shape space. (For our three-link swimmer, only the first Lie bracket is required for most points in shape space, and then one checks that second-order brackets span the remaining directions of $\mathfrak{se}(2)$ at degenerate points.) It is then possible to design small-amplitude gaits to achieve group trajectory tracking following a constructive procedure similar to that in [11].

As an example of an application of the curvature plots for non-Abelian Lie groups, we develop a gait to achieve pure net lateral motion, that is, so that the fish swims "sideways." Consider the contour plot of the v component of curvature in Figure 15. Superimposed on this plot are the zero-value contours of both the ω and u curvature components, in blue and magenta, respectively. At the intersection of these two zero-value contours, only the v curvature component is nonzero. A closed path taken about this point, as depicted with a black curve, results in nearly pure net sideways motion of the fish. The net motion will approach a pure lateral direction as the area enclosed by the path approaches zero.

5. Motion planning. Motivated by cross-sectional plots of Figure 14, we consider a family of gaits to develop a method for tracking a desired trajectory. In particular, we focus on gaits in which the displacement per gait period is small compared to the overall desired trajectory displacements. We find that a circular path in shape space about the origin results in pure net forward motion. From the ω curvature plot in Figure 4 and from the cross-sectional plot in Figure 14, we see that shifting the gait away from the origin along the line $\theta_1 = -\theta_2$ increases

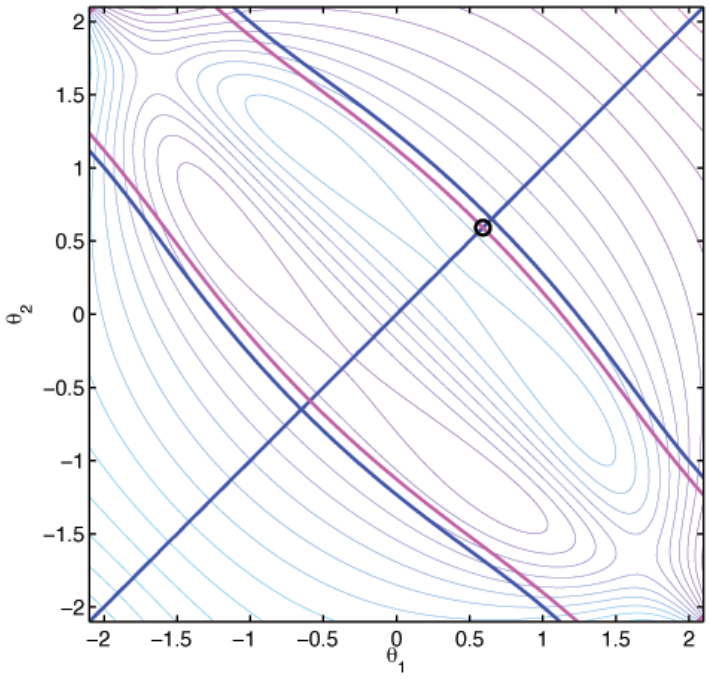

Figure 15. *Contour lines of the v curvature component, with the zero-value contours of the ω and u curvature components in blue and magenta, respectively. A gait represented by a black curve at the intersection of the two zero-value contours results in nearly pure net lateral motion.*

the net rotation. From numerical experiments we find that the net motion is a rotation plus a displacement.

The gait $(\theta_1(t), \theta_2(t))$ is given by the rapidly oscillating complex-valued function

$$\theta(t) = \theta_1(t) + i\theta_2(t) = Ae^{i\omega t} + B(t)(1-i). \tag{5.1}$$

The slowly varying offset B corresponds to shifting the circular trajectory about the line $\theta_1 = -\theta_2$. Here we choose $B(t)$ so that the body follows a desired trajectory in the plane. We hold A, the amplitude of the path, fixed. We perform numerical experiments to compute the displacement δ and rotation β from the forward direction (which is defined as the direction in which the body moves for $B = 0$) over a single period T of oscillation, as functions of B. The average velocity and curvature are given by

$$\langle v\rangle(B) = \frac{\delta}{T} = \frac{\omega\delta(B)}{2\pi}, \qquad \langle \kappa\rangle(B) = \frac{2\sin\left(\frac{\beta(B)}{2}\right)}{\delta(B)}. \tag{5.2}$$

For a fixed value of A, we compute $\langle v\rangle$ and $\langle\kappa\rangle$ for several values of B, a polynomial fit is applied, and finally the inverse function, $B = P(\langle\kappa\rangle)$, is found. We want to follow a specified trajectory, $r(t) = (x(t), y(t))$, where the velocity and curvature along the path are given by

$$v(t) = \sqrt{\dot{x}^2 + \dot{y}^2}, \qquad \kappa(t) = \frac{\dot{x}\ddot{y} - \dot{y}\ddot{x}}{(\dot{x}^2 + \dot{y}^2)^{3/2}}. \tag{5.3}$$

Since $B(t)$ is slowly varying (sometimes referred to as an adiabatic approximation), we ignore the contribution of $\dot{B}$ to $\dot{\theta}$. We match $\langle v \rangle(\omega, B) = v(t)$ and $\langle \kappa \rangle(B) = \kappa(t)$ and solve for ω and B as functions of time:

$$B(t) = P(\kappa), \qquad \omega(t) = 2\pi \frac{v}{\delta(B)}. \tag{5.4}$$

Finally, the prescribed path in shape space to approximately track the desired trajectory is

$$\theta(t) = Ae^{i\int_0^t \omega(t')dt'} + B(t)(1-i). \tag{5.5}$$

This method works well only for smoothly varying trajectories where the displacement per gait period is small compared to the dimension of the trajectory. Figure 16 shows the desired path in black along with the actual path in blue due to prescribing open loop controls. An animated video shows the shape deformations as the body follows the desired path.

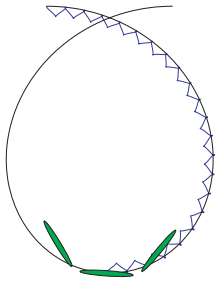

Figure 16. *The desired and actual trajectories in black and blue, respectively, resulting from open-loop controls based on the adiabatic approximation. See also the accompanying animation* (64988_03.gif [841KB]).

6. Conclusions. We have considered the swimming of an articulated fish-like swimming mechanism in a two-dimensional potential flow. We have extended the geometric theory to apply previously known results for systems on Abelian groups to the rotation component of $SE(2)$, exploiting the semidirect product structure. Using plots of the curvature of the local connection form, we developed gaits to achieve a desired rotation for a three-link swimmer. It was found that the most efficient turning gaits correspond to "C"-shaped configurations of the body. A parametric study was performed to assess the degree of maneuverability of different geometries, and it was found that large aspect ratio links with large gaps between the joints result in larger curvature values and are better suited for rotational maneuvering. The curvature plots were used to validate the hydrodynamically decoupled assumption used in previous works and to study the difference between two-link and three-link swimmers. It was shown that removing the middle link can improve the turning gait motion for some gaits. Although the main result is not applicable to non-Abelian groups in general, the curvature plots can be used to develop small-amplitude gaits to follow a desired trajectory. Finally, motivated by the cross section of the ω curvature plot, we considered a family of finite-amplitude gaits and developed a method for tracking a desired trajectory in the plane.

Acknowledgments. We wish to thank Scott Kelly, Jerry Marsden, and Eva Kanso for their insights and conversations on the subject of this paper, and George Lauder for biological inspiration and for providing the photo in Figure 10. We also thank the anonymous referee for the many helpful remarks.

REFERENCES

[1] H. Cendra, J. E. Marsden, and T. S. Ratiu, *Lagrangian reduction by stages*, Mem. Amer. Math. Soc., 152 (2001).
[2] E. G. Drucker and G. V. Lauder, *Locomotor function of the dorsal fin in teleost fishes: Experimental analysis of wake forces in sunfish*, J. Exp. Biol., 204 (2001), pp. 2943–2958.
[3] E. G. Drucker and G. V. Lauder, *Wake dynamics and fluid forces of turning maneuvers in sunfish*, J. Exp. Biol., 204 (2001), pp. 431–442.
[4] E. Kanso, J. E. Marsden, C. W. Rowley, and J. B. Melli-Huber, *Locomotion of articulated bodies in a perfect fluid*, J. Nonlinear Sci., 15 (2005), pp. 255–289.
[5] S. D. Kelly, *The Mechanics and Control of Robotic Locomotion with Applications to Aquatic Vehicles*, Ph.D. thesis, California Institute of Technology, Pasadena, CA, 1998.
[6] S. D. Kelly and R. M. Murray, *Modelling efficient pisciform swimming for control*, Internat. J. Robust Nonlinear Control, 10 (2000), pp. 217–241.
[7] G. Kirchhoff, *Ueber die bewegung eines rotationskörpers in einer flüssigkeit*, Crelle, 71 (1869), p. 237.
[8] P. S. Krishnaprasad and R. Yang, *Geometric phases, anholonomy, and optimal movement*, in Proceedings of the IEEE Conference Robotics and Automation, Volume 3, IEEE Robotics and Automation Society, Sacramento, CA, 1991, pp. 2185–2189.
[9] H. Lamb, *Hydrodynamics*, Dover, New York, 1945.
[10] G. V. Lauder and E. D. Tytell, *Hydrodynamics of undulatory propulsion*, in Fish Biomechanics, Fish Physiology 23, R. E. Shadwick and G. V. Lauder, eds., Academic Press, San Diego, 2006, pp. 425–468.
[11] N. E. Leonard and P. S. Krishnaprasad, *Motion control of drift-free, left-invariant systems on Lie groups*, IEEE Trans. Automat. Control, 40 (1995), pp. 1539–1554.
[12] M. J. Lighthill, *Note on the swimming of slender fish*, J. Fluid Mech., 9 (1960), pp. 305–317.
[13] M. J. Lighthill, *Hydrodynamics of aquatic animal propulsion*, Ann. Rev. Fluid Mech., 1 (1969), pp. 413–446.
[14] M. J. Lighthill, *Aquatic animal propulsion of high hydromechanical efficiency*, J. Fluid Mech., 44 (1970), pp. 265–301.
[15] M. J. Lighthill, *Large-amplitude elongated-body theory of fish locomotion*, Proc. Roy. Soc. London B, 179 (1971), pp. 125–138.
[16] W. Magnus, *On the exponential solutions of differential equations for a linear operator*, Comm. Pure Appl. Math., 7 (1954), pp. 649–673.
[17] J. E. Marsden and T. S. Ratiu, *Introduction to Mechanics and Symmetry*, Texts Appl. Math. 17, 2nd ed., Springer-Verlag, New York, 1999.
[18] J. E. Marsden, T. Ratiu, and A. Weinstein, *Semidirect products and reduction in mechanics*, Trans. Amer. Math. Soc., 281 (1984), pp. 147–177.
[19] J. E. Marsden, *Lectures on Mechanics*, London Math. Soc. Lecture Note Ser. 174, Cambridge University Press, Cambridge, UK, 1990.
[20] J. E. Marsden, R. Montgomery, and T. S. Ratiu, *Reduction, symmetry, and phases in mechanics*, Mem. Amer. Math. Soc., 88 (436) (1990).
[21] R. Mason and J. W. Burdick, *Propulsion and control of deformable bodies in an ideal fluid*, in Proceedings of the IEEE International Conference on Robotics and Automation, Detroit, MI, 1999, pp. 773–780.
[22] J. E. Radford, *Symmetry, Reduction and Swimming in a Perfect Fluid*, Ph.D. thesis, California Institute of Technology, Pasadena, CA, 2003.

[23] J. E. Radford and J. W. Burdick, *Local motion planning for nonholonomic control systems evolving on principal bundles*, in Proceedings of the International Symposium on Mathematical Theory of Networks and Systems, Padova, Italy, 1998.
[24] T. Y. Wu, *Swimming of a waving plate*, J. Fluid Mech., 10 (1961), pp. 321–344.
[25] T. Y. Wu, *Hydrodynamics of swimming propulsion. Part* 1. *Swimming of a two-dimensional flexible plate at variable forward speeds in an inviscid fluid*, J. Fluid Mech., 46 (1971), pp. 337–355.